

---

# Capability $\neq$ Interpretability: Human Interpretability of Vision Foundation Models

---

**Julien Colin**  
ELLIS Alicante, Spain  
Brown University, USA  
julien\_colin@brown.edu

**Lore Goetschalckx**  
imec, Leuven, Belgium

**Nuria Oliver\***  
ELLIS Alicante, Spain

**Thomas Serre\***  
Brown University, USA

## Abstract

How interpretable are the features of leading vision models? The question is increasingly pressing as these models move from research benchmarks into high-stakes deployments, yet existing methods cannot answer it reliably. We close this gap with a framework for measuring and comparing the human interpretability of vision models, built around two complementary psychophysics protocols: (1) *localizability*—can an observer predict *where* a feature fires on a novel image?—and (2) *nameability*—can an observer accurately describe *what* the feature represents? Features are recovered via sparse autoencoders, and a chance-anchored scoring function places every model on a common scale. Applying the framework to six vision transformers—two supervised ViTs and four foundation models (DINOv2, DINOv3, CLIP, SigLIP)—we collected more than 15,000 behavioral responses, analyzing the 13,400 responses from the 377 participants who passed our pre-specified quality checks. Foundation models are consistently *less* interpretable than their supervised counterparts, and the gap is not a capability tradeoff: interpretability does not correlate with downstream task performance on any benchmark we examine. What does correlate is the *locality* of a feature’s activations and *coarse-grained* semantic alignment with humans—models with focal activations and representations that reflect the world’s broad categorical structure produce more interpretable features, whereas fine-grained perceptual alignment does not. The two protocols yield strongly correlated rankings and share the same predictors, establishing interpretability as an independent, measurable dimension of representation quality—and, surprisingly, one on which every foundation model we tested falls below the supervised baselines that came before. Capability alone cannot close that gap; locality and coarse-grained alignment can.

## 1 Introduction

The dominant paradigm in modern computer vision is to pretrain large foundation models and fine-tune them for specific tasks. Built on the vision transformer [1], models like CLIP [2], SigLIP [3], DINOv2 [4], and DINOv3 [5] already serve as general-purpose visual backbones across an ever-expanding range of downstream tasks, including classification [6], segmentation [7], object tracking [8, 9], and robotic perception [10]. The same models are increasingly deployed in high-stakes settings—clinical decision support [11–14], autonomous driving [15, 16]—where a user often needs

---

\*co-principal investigators

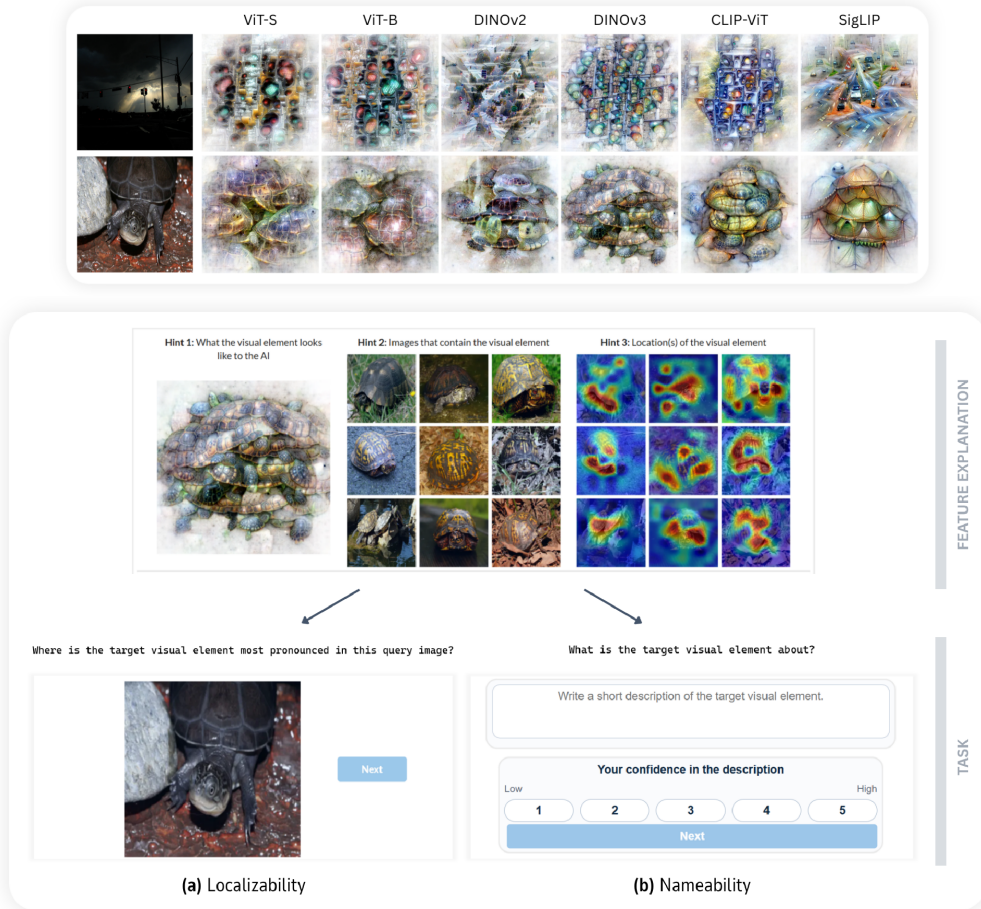


Figure 1: Models trained under different objectives learn different internal representations and, consequently, different features. Which of these features are more interpretable to humans remains an open question. **Top:** the most important feature recovered by each of the six models we study, for the prediction of *traffic light* (first row) and *mud turtle* (second row). **Bottom:** Our framework, illustrated for DINOv3. Given a feature and its visual explanation—a synthetic visualization, highly activating images, and corresponding heatmaps showing where the feature fires (top panels)—participants either click where they think the feature fires on a novel image (left, *localizability*) or describe what the feature represents in free text (right, *nameability*).

to understand what a model is actually responding to. How interpretable, then, are the features that today’s leading vision models have learned?

Surprisingly little work compares vision models on this dimension, because existing evaluation protocols cannot place different models on a common, reliable scale of feature interpretability (Section 2).

To fill this gap, we introduce a model evaluation framework comprising two psychophysics protocols that quantify two complementary dimensions of feature understanding: feature *localizability* — can an observer predict *where* a feature fires on a novel image? — and feature *nameability* — can an observer accurately describe *what* a feature represents? Together they form a comprehensive evaluation (see Fig. 1, bottom): a feature can fire in a predictable location yet defy verbal description, or be easy to name yet hard to point to. The proposed framework has three properties that enable a fair cross-model comparison: (i) it replaces the polysemantic neuron basis used in prior work with monosemantic directions recovered via sparse autoencoders [17, 18], so each tested unit corresponds to a single concept; (ii) it evaluates *functionally analogous* features across models by anchoring feature selection to a shared set of input images (Fig. 1, top), rather than sampling features randomly

from each model; and (iii) it uses calibrated scores to a common chance level across features and models, so raw scores are directly comparable. Furthermore, the evaluation is scaled to  $\sim 6,000$  features across six models at a fraction of the cost of previous protocols [19].

We apply the framework to six vision transformers—two supervised ViTs and four foundation models (DINOv2 [4], DINOv3 [5], CLIP [2], SigLIP [3])—and collect more than 15,000 behavioral responses, of which the 13,400 from the 377 participants who passed our pre-specified quality checks enter the analyzes. The headline finding is sobering: every foundation model we tested produces features that are *less* interpretable than those of the supervised baselines that came before, and downstream task performance does not predict the gap. Two representational properties do: feature *locality* and *coarse-grained* semantic alignment with human similarity judgments. DINOv3—whose training objective explicitly promotes local features—is the encouraging counterexample, suggesting that the gap is not architectural destiny.

Our contributions are: **(1)** a framework for measuring and comparing the human interpretability of vision models, with two complementary psychophysics protocols—*localizability* and *nameability*; **(2)** a human study across six vision transformers showing that every foundation model we tested produces features that are *less* interpretable than those of the supervised baselines that came before, yet this gap is not a consequence of their greater capability: downstream performance does not explain it; and **(3)** the identification of two representational properties that predict interpretability—*locality* of feature activations and *coarse-grained* semantic alignment with humans.

## 2 Related Work

**Sparse autoencoders and monosemanticity.** Under the superposition hypothesis [20], networks encode more features than they have neurons by superimposing concepts onto shared activation channels, producing polysemantic neurons. Sparse autoencoders (SAEs) recover a dictionary of monosemantic directions and have emerged as the dominant remedy [17, 18, 21, 22]. We extract features via SAEs to avoid the polysemy that complicates neuron-level analysis.

**Evaluation of model interpretability.** Bau et al. [23] introduced Network Dissection, to our knowledge the first framework to compare interpretability across models (architectures and training regimes). They score every convolutional unit from four CNNs against pixel-level masks from a set of human-labeled concepts (Broden), and models are ranked by the number of units that align with a concept above a given threshold. The approach is bounded by Broden’s vocabulary, restricted to the neuron basis, and conflates concept alignment with interpretability—which, as Section 4.2 shows, do not necessarily coincide.

Borowski et al. [24] pioneered psychophysics-based evaluation of DNN interpretability: participants viewed maximally and minimally activating images for a given neuron, then identified which of two novel query images also strongly activated it. Zimmermann et al. [19] scaled this protocol across nine vision and vision-language architectures (80 features per model, 720 in total—a small fraction of the thousands a typical model encodes) and concluded that more capable models are not necessarily more interpretable. Zimmermann et al. [25] later automated the evaluation by replacing human judgments with pairwise perceptual similarity. Their metric correlates with human results, but cross-model differences arise primarily from a tail of highly uninterpretable units linked to superposition. Applying a similar protocol to CNNs, Colin et al. [26] showed that reliance on a neuron basis can mask cross-model differences because the impact of superposition is itself model-specific. Two methodological limitations, therefore, prevent fair cross-model comparison in this lineage: exclusive reliance on the polysemantic neuron basis and a forced-choice task whose process-of-elimination shortcuts produce model-specific chance levels. Our framework resolves both and extends model coverage to several foundation models that postdate prior studies.

## 3 Method

### 3.1 Current protocols are ill-suited for model interpretability.

Prior protocols [19, 24] frame the task as a contrastive forced-choice: participants view maximally and minimally activating images for a feature, then select which of two novel query images also strongly activates it (see Fig. A.1 in Appendix C for an example trial). While intuitive, this design

has a fundamental confound: participants can identify the correct answer by understanding what the feature is not about—*e.g.*, not a corn detector (Fig. A.1)—rather than genuinely interpreting the feature itself.

To test whether this confounding effect is consequential, we performed a control experiment on two models from Zimmermann et al. [19] (ResNet-50 and ViT-B32). We ran two versions of a given trial: the original version (Fig. A.1) and a variation where we replaced the maximally activating images with images ranking 25,000 out of 50,000 in each feature’s activation distribution, thus carrying little to no information about the feature’s visual content (Fig. A.2). In this case, participants were expected to perform at chance (50%). Instead, participants reliably exceeded chance with *model-specific baselines*: 53% for ViT-B32 and 60% for ResNet-50.

This model-specific baseline inflation makes raw accuracy scores incomparable across architectures. Zimmermann et al. [19] reported ResNet-50 as more interpretable than ViT-B32 (83% vs. 80%). However, once each score is expressed relative to its model-specific baseline, the ranking *reverses*: ViT-B32 is 27% above its baseline while ResNet-50 is only 23% above its own. Any protocol that does not account for this artifact risks drawing erroneous conclusions.

### 3.2 Framing interpretability as identification.

**Overview.** We address the limitations described above with a framework comprising of two complementary protocols that operationalize interpretability: *localizability*, *i.e.*, can a participant predict *where* a feature fires on a novel image?; and *nameability*, *i.e.*, can a participant accurately describe *what* a feature represents? Both protocols share the same feature extraction pipeline (Fig. A.3 in Appendix E) and the same visual explanations presented to participants (Fig. 1). They differ only in the task and scoring function. Because there is no distractor to exploit, participants must rely on genuine understanding of the feature’s visual content to perform. Localizability scores are mapped to a common chance-anchored scale (Section 3.2), enabling direct comparison across features, models and protocols. Nameability requires no chance-level correction: images and descriptions vary across models, but they are scored in a shared embedding space, making cross-model comparisons fair.

By evaluating the interpretability of features, we aim to derive a more general score representative of model interpretability. Whereas Zimmermann et al. [19] studied features across multiple layers, our focus on foundation models leads us, moving forward, to examine only the last latent representation of each model, *i.e.*, the output of the penultimate layer for supervised models, the output of the last layer for DINO models, and the output of the vision encoder for VLMs.

**Feature extraction.** For each model, we extract features from its vision encoder. Because individual neurons in vision models are often polysemantic [20], we use sparse autoencoders (SAEs) to recover a dictionary of monosemantic directions. TopK SAEs [18] are trained on activations from the ImageNet training split ( $\approx 1.28\text{M}$  images), using all patch tokens per image (256 for patch size 14 in DINOv2, 196 for patch size 16 in all other models). Each SAE uses an expansion factor of  $\times 10$ , yielding 3,840 features for ViT-S and 7,680 features from all the other models.

**Feature relevance and linear probing.** For each model, we train a linear classification head on ImageNet on top of the frozen backbone, from which we derive (i) per-feature importance scores that quantify each feature’s contribution to the classifier’s predictions, computed as Gradient input [27], shown to be particularly faithful in latent space [28]; and (ii) a downstream accuracy baseline used in Section 4.1.

**Feature selection.** Given that current computer vision models are expected to encode thousands of features, we aim to scale the number of features evaluated. Building on Zimmermann et al. [19], we first ran a pilot with 80 features and 10 trials per feature to obtain reliable per-feature interpretability estimates and a model interpretability score. We then evaluated the depth-vs-breadth tradeoff: we found that the number of features evaluated is more important than the number of repetitions per feature to obtain stable model-level estimates (see Appendix D). We therefore adopted this design in the main experiment.

Following common practice [29, 30], we exclude dense features—*i.e.*, SAE features that activate on most inputs and do not encode specific concepts—leaving between 500 and 1,300 unique features per model, which reflects architectural differences in feature reuse (see Appendix F).

**Feature explanation.** Both protocols present participants with the same visual explanation of a feature (Fig. 1- top): (a) a synthetic feature visualization synthesized via MACO [31] that maximally activates the feature (left panel in Fig. 1); (b) nine highly activating natural images (middle panel in Fig. 1); and (c) their corresponding RISE heatmaps [32] indicating where the feature fires on each image (right panel in Fig. 1). Participants use these three sources of information to form an understanding of the feature before solving the task.

**Localizability (where).** Each *localizability* trial additionally presents (d) a novel query image (bottom, left in Fig. 1) and participants are asked to click on the region of the image where they believe the feature appears. Each click is scored against the RISE heatmap of the query image (smoothed with a Gaussian filter) as follows.

Let  $v$  be the heatmap value at the clicked location and  $p = \widehat{F}(v)$  its empirical cumulative distribution function (ECDF) over the heatmap pixels. Because heatmap distributions vary across features (*e.g.*, sparse vs. diffuse activations), raw percentiles are not directly comparable across features or models. We therefore introduce a *chance-anchored normalization* that pins chance to  $s = 0.5$ . Writing  $p_\mu = \widehat{F}(\mu)$  for the percentile rank of the mean activation  $\mu$ , we map  $p_\mu$  to 0.5 and the extremes to 0 and 1:

$$s(v) = \begin{cases} 0.5 - 0.5 \cdot \frac{p_\mu - p}{p_\mu}, & \text{if } p < p_\mu, \\ 0.5 + 0.5 \cdot \frac{p - p_\mu}{1 - p_\mu}, & \text{otherwise.} \end{cases}$$

By pinning chance ( $s = 0.5$ ) to the mean activation, the score carries the same interpretation across features and models — a click above the mean scores above chance, below the mean scores below—regardless of whether the feature activates focally or diffusely. We refer to this score as the *localizability* score.

**Nameability (what).** Each *nameability* trial asks participants (d) to write a short free-text description of the feature (bottom, right in Fig. 1), based on the explanation panel shown at the top, and a confidence score about their description on a 5-point Likert scale. We aim to collect multiple descriptions per feature, which scales up the number of trials per feature. We compensate this increase by evaluating a representative subsample rather than the full feature set: for each model, we bin features into deciles by their *localizability* score and sample uniformly within each bin ( $\sim 30$  features per 10% bin,  $\sim 300$  features per model).

We score the description by comparing it against the feature’s visual content in CLIP’s joint vision–language space [2]. For each of the nine most-activating images, we take a  $96 \times 96$  crop centered on the peak RISE activation ( $\sim 1/5$  of the image) and encode it with the CLIP image encoder. We encode the participant’s description with the CLIP text encoder. The *nameability* score is the mean cosine similarity between the text embedding and the nine crop embeddings.

Note that we compare against *crops* rather than whole images so the score rewards descriptions that go beyond naming the object, something that does not necessarily emerge when using the full image (Fig. A.9). Regardless, the results are robust to using the full image (see Appendix I).

Due to the CLIP modality gap, *nameability* scores are bounded well below 1. In practice, they range between 0.13 and 0.35 with a chance-level of 0.19—average similarity for an image-text pair sampled from two different features. See Appendix I for further details.

**Participants.** Across both experiments, we recruited about 440 participants via Prolific<sup>2</sup>. All were native English speakers without reported visual impairments and completed the study on a laptop or desktop. Each provided informed consent and received \$2.95 ( $\sim$ \$16/hr; 10–13 minutes). The protocol was approved by the IRB of an author-affiliated institution. We analyze about 13,400 behavioral responses from the 377 participants who (i) passed at least 4 of 6 practice trials, (ii) answered all 4 attentiveness catch trials correctly, and (iii) completed the experiment within 3 SDs of the mean duration.

<sup>2</sup>[www.prolific.com](http://www.prolific.com)

## 4 Results

We evaluated six vision transformers: two supervised baselines (ViT-S/16 and ViT-B/16) and four foundation models—DINOv2 ViT-B/14, DINOv3 ViT-B/16, CLIP ViT-B/16, and SigLIP ViT-B/16.

Table 1: Localizability, Nameability and Confidence scores across six vision transformers. Supervised models consistently outperform foundation models on both dimensions. Best result per row is in bold, second best is underlined.

	Supervised		Foundation			
	ViT-S	ViT-B	DINOv2	DINOv3	CLIP	SigLIP
Localizability ( $\uparrow$ )	80.3	<b>86</b>	71	80	79.7	71.4
Nameability ( $\uparrow$ )	<b>0.274</b>	<u>0.273</u>	0.259	0.260	0.266	0.253
Confidence ( $\uparrow$ )	3.43	<u>3.61</u>	<b>3.68</b>	3.41	3.51	3.38

**Foundation models are less interpretable than supervised ones.** We measure interpretability with both the *localizability* and the *nameability* scores<sup>3</sup>, reflected in Table 1. Localizability ( $L$ ) and *nameability* ( $N$ ) scores differ significantly across models ( $L$ : Kruskal–Wallis,  $H(5) = 118.40$ ,  $p < .001$ ;  $N$ : Kruskal–Wallis,  $H(5) = 295.36$ ,  $p < .001$ ). As seen in the table, foundation models are consistently less interpretable than their supervised counterparts (Dunn’s test and Tukey HSD’s test,  $p < .001$  vs. ViT-B), regardless of whether they were trained with language supervision (CLIP, SigLIP) or pure self-supervised objectives (DINOv2, DINOv3). Moreover, while we expect *localizability* and *nameability* to quantify two different dimensions of interpretability, in practice we find that they are highly correlated ( $r=0.84$ ,  $p=0.036$ ; Fig. A.14). Qualitative examples spanning the four quadrants of *localizability* and *nameability* are shown in Appendix Fig. A.8.

**Models can feel more interpretable than they are.** Average confidence is fairly homogeneous across models (3.38 – 3.68, Table 1, bottom row), but its alignment with interpretability is not. While DINOv2 elicits the highest confidence and ranks near the bottom on interpretability (last on *localizability*, second-to-last on *nameability*), SigLIP performs poorly on all fronts. Based on these results, a model can feel more interpretable than it is—see Appendix Fig. A.7 for examples of features that are confidently but inaccurately named (and vice versa), a caution worth keeping in mind given that DINOv2 features have been treated as a reference for interpretable representations [33].

### 4.1 Alignment with performance

A natural question is whether interpretability and capability are linked: models with richer, more semantically structured representations might be both more capable on downstream tasks and more legible to humans. We measured the Spearman correlation between each model’s interpretability scores and its performance on three vision tasks: ImageNet-1k classification, semantic segmentation, and perceptual grouping. We report those results in Fig. 2.

**ImageNet-1k classification.** Foundation models lead on ImageNet top-1 accuracy but trail on interpretability. Across the six models, neither *localizability* ( $\rho = -0.48$ ,  $p = 0.33$ ) nor *nameability* ( $\rho = -0.6$ ,  $p = 0.21$ ) correlate significantly with classification (Fig. 2). DINOv2 and SigLIP match CLIP on accuracy yet score roughly 8 points lower in *localizability*.

**Semantic segmentation.** Segmentation performance on ADE20K[34]—using a linear probe<sup>4</sup>—does not correlate significantly with either *localizability* ( $\rho = -0.54$ ,  $p = 0.27$ ) or with *nameability* ( $\rho = -0.77$ ,  $p = 0.07$ ).

<sup>3</sup>For both measures, we report the median per model as scores do not follow a normal distribution, see Appendix J

<sup>4</sup>We follow the DINOv3 methodology but force all models to an input size of  $224 \times 224$ , since supervised ViTs from `timm` cannot take flexible input sizes. The same pipeline at  $512 \times 512$  reproduces DINOv3 results.

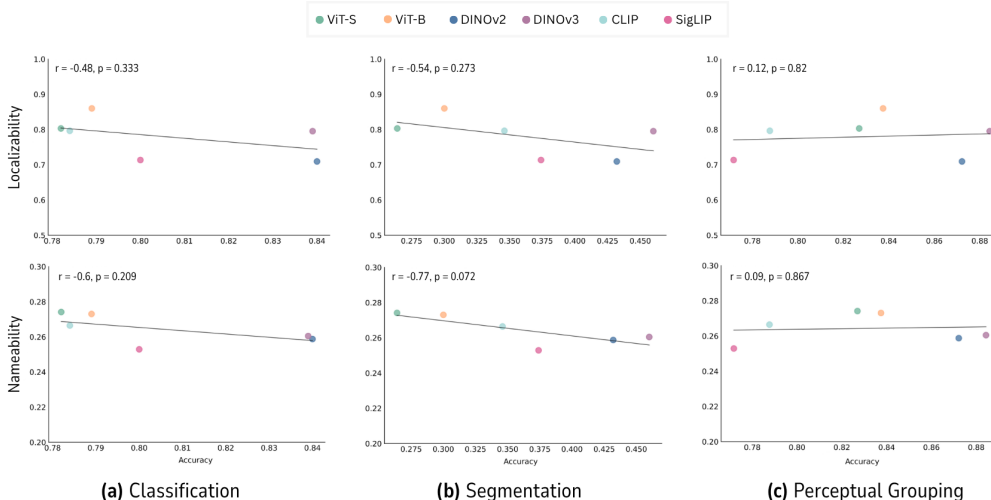


Figure 2: **Interpretability is uncorrelated with downstream task performance.** Each panel plots an interpretability score against a capability benchmark across the six models. Top row: *localizability*; bottom row: *nameability*. Columns: ImageNet-1k top-1 accuracy, ADE20K semantic segmentation, and perceptual grouping. Spearman  $\rho$  and  $p$ -values are shown in each panel. Correlations are non-significant for both interpretability measures across all three benchmarks, suggesting that interpretability and downstream task performance capture largely orthogonal properties of a visual representation.

**Perceptual grouping.** On a perceptual grouping benchmark—a more constrained form of segmentation that probes the models’ ability to bind individual object instances—we again find no significant correlation with either *localizability* ( $\rho = 0.12$ ,  $p = 0.82$ ) nor *nameability* ( $\rho = 0.09$ ,  $p = 0.87$ ; Fig. 2).

Across all three benchmarks, task performance does not predict interpretability. This dissociation suggests that the representational properties that make a model useful for downstream tasks are largely orthogonal to those that make its features interpretable to humans.

**Locality of the representation.** Beyond task performance, we ask whether *locality*, *i.e.*, the degree to which a feature’s activations concentrate on confined image regions, predicts interpretability: a focal activation supplies a concrete spatial anchor (an object part, a texture), while a diffuse one leaves the participant to guess what the activating regions share. We quantify locality with the Hoyer metric applied to each feature’s RISE heatmaps [35]:

$$H(\mathbf{x}) = \frac{(\sqrt{n} - \|\mathbf{x}\|_1 / \|\mathbf{x}\|_2)}{(\sqrt{n} - 1)}$$

with  $n$  the number of pixels, and where  $H = 0$  corresponds to uniform activation across the image and  $H = 1$  to all mass on a single pixel. We average  $H$  across each feature’s 9 most activating images and then across the model’s features. In contrast to task performance, locality correlates strongly with *localizability* ( $\rho = 0.91$ ,  $p = 0.01$ ; Fig. 3, top left) and *nameability* ( $\rho = 0.99$ ,  $p < .001$ ; Fig. 3, bottom left). See Appendix K for additional results.

## 4.2 Alignment with human perception

Next, we consider human alignment, *i.e.*, the degree to which a model aligns with some properties of human perception, as alignment has been shown to improve representation quality over a wide range of downstream tasks [36–39]. Because not all measures of alignment capture the same properties of human perception [40], we study 3 kinds of alignment: alignment with human (a) visual strategies; (b) coarse-grained similarity judgments (semantic similarity); and (c) fine-grained similarity judgments (lower-level visual similarity).

**Alignment with human visual strategies.** Strategy alignment—the overlap between model-driven and human-attended image regions [41, 42]—does not correlate significantly with *localizability* ( $\rho = 0.14, p = 0.8$ ; Fig. A.15, left) or *nameability* ( $\rho = 0.21, p = 0.7$ ; Fig. A.15, right).

**Alignment with human similarity judgments.** Human similarity judgments operate at multiple levels of abstraction [39]. *Fine-grained* similarity captures within-category distinctions (e.g., how similar two butterfly species are to each other), while *coarse-grained* similarity captures broad semantic structure across categories (e.g., how similar a buffalo is to a spider relative to grass). We measure alignment at the different levels of similarity using three datasets: THINGS similarity [43, 44], Levels [39], and NIGHTS [38, 45].

Alignment with *fine-grained* similarity does not correlate with neither *localizability* (NIGHTS:  $\rho = -0.41, p = 0.42$ ; Levels:  $\rho = 0.16, p = 0.76$ ; Fig. A.16, top row) nor *nameability* (NIGHTS:  $\rho = -0.47, p = 0.35$ ; Levels:  $\rho = 0.26, p = 0.62$ ; Fig. A.16, bottom row). In contrast, alignment with *coarse-grained* similarity is generally lower and shows a strong correlation with interpretability (Fig. 3, middle and right), which is significant for the THINGS similarity dataset: *localizability* (THINGS:  $\rho = 0.84, p = 0.04$ , Levels:  $\rho = 0.71, p = 0.11$ ) and *nameability* (THINGS:  $\rho = 0.85, p = 0.03$ ; Levels:  $\rho = 0.6, p = 0.21$ ). See Appendix L for additional results.

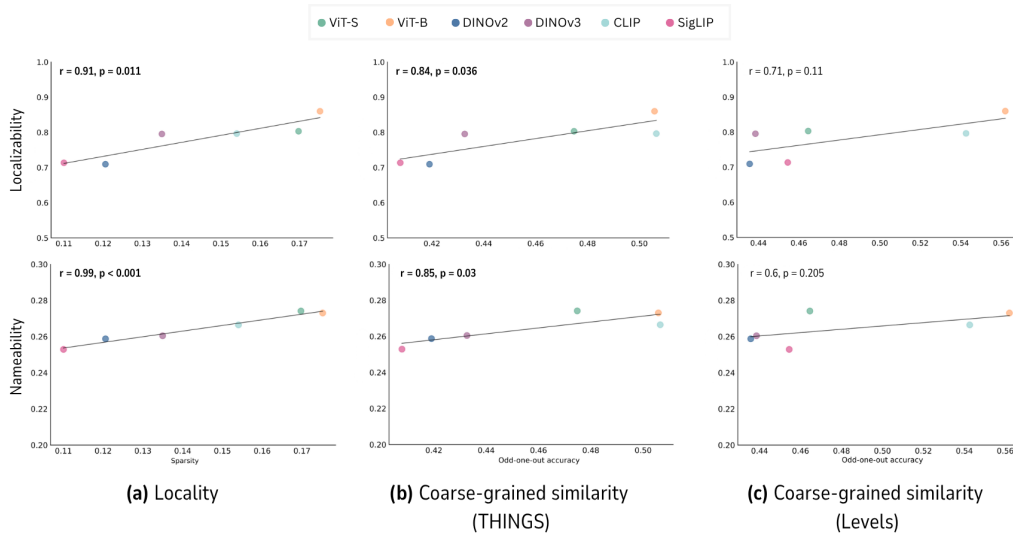


**Figure 3: Locality and coarse-grained semantic alignment track interpretability.** Each panel plots an interpretability score against a representational property across the six models. Top row: *localizability*; bottom row: *nameability*. Columns: locality of the representation (mean Hoyer sparsity over feature heatmaps), and coarse-grained alignment with human similarity judgments on THINGS [43] and Levels [39] (odd-one-out accuracy). Spearman  $\rho$  and  $p$ -values per panel. Locality is the strongest predictor of interpretability, consistent with focal activations providing a clearer visual anchor for understanding a feature. Coarse-grained alignment also tracks interpretability, particularly on THINGS, suggesting that interpretable representations are not only local but also organized in ways that better reflect human categorical similarity judgments.

This dissociation between granularity levels suggests that what matters for interpretability is not perceptual fidelity to fine visual detail, but rather the degree to which a model organizes its features around the same high-level semantic categories that structure human perception. A feature that groups concepts according to what humans consider broadly similar is more likely to be a feature that humans can understand.

## 5 Discussion

**Two protocols, one interpretability.** The two protocols differ in nearly every respect: one asks participants to point, the other to write; one is scored against a spatial heatmap, the other against a vision–language embedding. That they yield concordant rankings and surface the same predictors is

unlikely to be coincidence—we appear to be measuring a stable property of the representations rather than an artifact of any one task, and either protocol may suffice on its own in future work.

**Foundation models are less interpretable than their supervised counterparts.** The gap appears in both vision-only SSL models (DINOv2, DINOv3) and vision-language models (CLIP, SigLIP), so neither pretraining signal is the cause. The common factor is foundation-style pretraining itself. One reading is that these models reach—and on many benchmarks exceed—human performance in part by developing *superhuman* features: representations effective for the task but not the kind a human observer can readily make sense of. The very generality that makes foundation models capable may also push their representations away from a human-interpretable basis. This gap is easy to miss without direct evaluation—DINOv2, often treated as a reference for interpretable representations [33], elicits the highest rater confidence yet ranks among the least interpretable models on *localizability* and *nameability*.

**Interpretability is orthogonal to task performance.** Across every benchmark we examined, capability and interpretability are uncorrelated. The relationship is neither a tradeoff nor a free lunch: how well a model classifies, segments, or groups says little about whether a human can interpret its features. The leaderboards by which the field currently judges progress are silent on interpretability, a property independently desirable in high-stakes settings (*e.g.*, clinical decision support or autonomous driving) where these same backbones are increasingly considered. Interpretability has to be designed for explicitly; it will not arrive as a byproduct of capability, and prior evidence suggests that scale alone does not guarantee it either [19].

**Locality is the proximate signature of an interpretable representation.** The locality of feature activations is the strongest predictor of interpretability we identify. Foundation models tend to develop diffuse features that fire across larger, less focused regions, blending local content with broader scene context. This may help on downstream tasks but leaves a human observer without a clear visual anchor. DINOv3 is the encouraging exception: one of the most capable models in our set and also among the most interpretable foundation models, because its training objective explicitly promotes local features. This finding suggests that locality-aware objectives can partially close the interpretability gap, though whether they do so without capability cost requires additional direct experimental verification.

**Coarse-grained semantic alignment, not perceptual fidelity, predicts interpretability.** Of the alignment measures we considered, only coarse-grained alignment with human similarity judgments tracks interpretability. A model can attend to the same image regions humans do, yet still encode what it sees there in features humans cannot make sense of. Fine-grained perceptual alignment has been found to be uniformly high and largely shared across models [46]. Coarse-grained alignment, on the other hand, is consistently lower, leaving real room for improvement. Interpretability appears driven less by perceptual fidelity than by how a representation organizes the visual world at the categorical level. Training signals built from human odd-one-out judgments [43] seem like a promising direction to close part of the gap.

## 6 Conclusion

We introduced a framework for measuring and comparing the human interpretability of vision models, built around two complementary psychophysics protocols: *localizability* (where a feature fires) and *nameability* (what it represents). Across six vision transformers and more than 15,000 behavioral responses, foundation models, whether trained with language supervision or self-supervised objectives, were consistently *less* interpretable than their supervised counterparts—a surprising result for models that have surpassed those same baselines on most other axes. The gap is not a capability tradeoff: interpretability is uncorrelated with downstream task performance on every benchmark we examined, and the two structurally different protocols agree on this conclusion and on the predictors that drive it. Two properties track interpretability: the *locality* of a feature’s activations and *coarse-grained* semantic alignment with human similarity judgments. Together, they point to a concrete recipe for building more interpretable vision models—training objectives that promote local feature activations and align representations with the coarse semantic structure of human perception [39]—and DINOv3,

whose objective explicitly promotes locality, suggests that capability and interpretability need not trade off when locality is an explicit training objective.

## References

- [1] Alexey Dosovitskiy, Lucas Beyer, Alexander Kolesnikov, Dirk Weissenborn, Xiaohua Zhai, Thomas Unterthiner, Mostafa Dehghani, Matthias Minderer, Georg Heigold, Sylvain Gelly, Jakob Uszkoreit, and Neil Houlsby. An Image is Worth 16x16 Words: Transformers for Image Recognition at Scale. In *Proceedings of the International Conference on Learning Representations (ICLR)*, 2021. URL <https://openreview.net/forum?id=YicbFdNTTy>.
- [2] Alec Radford, Jong Wook Kim, Chris Hallacy, Aditya Ramesh, Gabriel Goh, Sandhini Agarwal, Girish Sastry, Amanda Askell, Pamela Mishkin, Jack Clark, et al. Learning transferable visual models from natural language supervision. In *Proceedings of the International Conference on Machine Learning (ICML)*, pages 8748–8763. PmLR, 2021.
- [3] Xiaohua Zhai, Basil Mustafa, Alexander Kolesnikov, and Lucas Beyer. Sigmoid loss for language image pre-training. In *Proceedings of the IEEE International Conference on Computer Vision (ICCV)*, pages 11975–11986, 2023.
- [4] Maxime Oquab, Timothée Darcet, Théo Moutakanni, Huy Vo, Marc Szafraniec, Vasil Khalidov, Pierre Fernandez, Daniel Haziza, Francisco Massa, Alaaeldin El-Nouby, et al. DINOv2: Learning robust visual features without supervision. *arXiv preprint arXiv:2304.07193*, 2023.
- [5] Oriane Siméoni, Huy V. Vo, Maximilian Seitzer, Federico Baldassarre, Maxime Oquab, Cijo Jose, Vasil Khalidov, Marc Szafraniec, Seungeun Yi, Michaël Ramamonjisoa, et al. DINOv3. *arXiv preprint arXiv:2508.10104*, 2025.
- [6] Christopher Chiu, Maximilian Heil, Teresa Kim, and Anthony Miyaguchi. Fine-grained classification for poisonous fungi identification with transfer learning. *arXiv preprint arXiv:2407.07492*, 2024.
- [7] Liu Shilong, Zeng Zhaoyang, Ren Tianhe, Li Feng, Zhang Hao, Yang Jie, Jiang Qing, Li Chunyuan, Yang Jianwei, Su Hang, Zhu Jun, and Lei Zhang. Grounding dino: Marrying dino with grounded pre-training for open-set object detection. *arXiv preprint arXiv:2303.05499*, 2024.
- [8] Niels G Faber, Seyed Sahand Mohammadi Ziabari, and Fatemeh Karimi Nejadasl. Leveraging foundation models via knowledge distillation in multi-object tracking: Distilling dinov2 features to fairmot. *arXiv preprint arXiv:2407.18288*, 2024.
- [9] Narek Tumanyan, Assaf Singer, Shai Bagon, and Tali Dekel. Dino-tracker: Taming dino for self-supervised point tracking in a single video. In *European Conference on Computer Vision*, pages 367–385. Springer, 2024.
- [10] Moo Jin Kim, Karl Pertsch, Siddharth Karamcheti, Ted Xiao, Ashwin Balakrishna, Suraj Nair, Rafael Rafailov, Ethan P Foster, Pannag R Sanketi, Quan Vuong, et al. Openvla: An open-source vision-language-action model. In *Conference on Robot Learning*, pages 2679–2713. PMLR, 2025.
- [11] Mohammed Baharoon, Waseem Qureshi, Jiahong Ouyang, Yanwu Xu, Abdulrhman Aljouie, and Wei Peng. Evaluating general purpose vision foundation models for medical image analysis: An experimental study of dinov2 on radiology benchmarks. *arXiv preprint arXiv:2312.02366*, 2023.
- [12] Théo Moutakanni, Piotr Bojanowski, Guillaume Chassagnon, Céline Hudelot, Armand Joulin, Yann LeCun, Matthew Muckley, Maxime Oquab, Marie-Pierre Revel, and Maria Vakalopoulou. Advancing human-centric ai for robust x-ray analysis through holistic self-supervised learning. *arXiv preprint arXiv:2405.01469*, 2024.
- [13] Licheng Jiao, Jiayao Hao, Ruiyang Li, Lingling Li, Xu Liu, Fang Liu, Wenping Ma, Puhua Chen, Zhongjian Huang, Jingyi Yang, Jiaxuan Zhao, and Qigong Sun. Foundation models meet medical image interpretation. *Research*, 9:1024, 2026. doi: 10.34133/research.1024. URL <https://spj.science.org/doi/abs/10.34133/research.1024>.
- [14] Tugba Akinci D’Antonoli, Christian Bluethgen, Renato Cuocolo, Michail E Klontzas, Andrea Ponsiglione, and Burak Kocak. Foundation models for radiology: fundamentals, applications, opportunities, challenges, risks, and prospects. *Diagnostic and Interventional Radiology*, 2025.

- [15] Haoxiang Gao, Zhongruo Wang, Yaqian Li, Kaiwen Long, Ming Yang, and Yiqing Shen. A survey for foundation models in autonomous driving. In *2025 6th International Conference on Computer Vision and Data Mining (ICCVDM)*, pages 63–71. IEEE, 2025.
- [16] Sicong Jiang, Zilin Huang, Kangan Qian, Ziang Luo, Tianze Zhu, Yang Zhong, Yihong Tang, Menglin Kong, Yunlong Wang, Siwen Jiao, et al. A survey on vision-language-action models for autonomous driving. In *Proceedings of the IEEE/CVF International Conference on Computer Vision*, pages 4524–4536, 2025.
- [17] Hoagy Cunningham, Aidan Ewart, Logan Riggs, Robert Huben, and Lee Sharkey. Sparse autoencoders find highly interpretable features in language models. *arXiv preprint arXiv:2309.08600*, 2023.
- [18] Leo Gao, Tom Dupré la Tour, Henk Tillman, Gabriel Goh, Rajan Troll, Alec Radford, Ilya Sutskever, Jan Leike, and Jeffrey Wu. Scaling and evaluating sparse autoencoders. *arXiv preprint arXiv:2406.04093*, 2024.
- [19] Roland S. Zimmermann, Thomas Klein, and Wieland Brendel. Scale alone does not improve mechanistic interpretability in vision models. *Advances in Neural Information Processing Systems (NeurIPS)*, 36, 2023.
- [20] Nelson Elhage, Tristan Hume, Catherine Olsson, Nicholas Schiefer, Tom Henighan, Shauna Kravec, Zac Hatfield-Dodds, Robert Lasenby, Dawn Drain, Carol Chen, Roger Grosse, Sam McCandlish, Jared Kaplan, Dario Amodei, Martin Wattenberg, and Christopher Olah. Toy models of superposition. *Transformer Circuits Thread*, 2022.
- [21] Adly Templeton, Tom Conerly, Jonathan Marcus, Jack Lindsey, Trenton Bricken, Brian Chen, Adam Pearce, Craig Citro, Emmanuel Ameisen, Andy Jones, Hoagy Cunningham, Nicholas L Turner, Callum McDougall, Monte MacDiarmid, C. Daniel Freeman, Theodore R. Sumers, Edward Rees, Joshua Batson, Adam Jermyn, Shan Carter, Chris Olah, and Tom Henighan. Scaling monosemanticity: Extracting interpretable features from claude 3 sonnet. *Transformer Circuits Thread*, 2024. URL <https://transformer-circuits.pub/2024/scaling-monosemanticity/index.html>.
- [22] Thomas Fel, Ekdeep Singh Lubana, Jacob S. Prince, Matthew Kowal, Victor Boutin, Isabel Papadimitriou, Binxu Wang, Martin Wattenberg, Demba E. Ba, and Talia Konkle. Archetypal SAE: Adaptive and stable dictionary learning for concept extraction in large vision models. In *Proceedings of the 42nd International Conference on Machine Learning*, volume 267 of *Proceedings of Machine Learning Research*, pages 16543–16572. PMLR, 2025.
- [23] David Bau, Bolei Zhou, Aditya Khosla, Aude Oliva, and Antonio Torralba. Network dissection: Quantifying interpretability of deep visual representations. In *Proceedings of the IEEE conference on computer vision and pattern recognition*, pages 6541–6549, 2017.
- [24] Judy Borowski, Roland S. Zimmermann, Judith Schepers, Robert Geirhos, Thomas S. A. Wallis, Matthias Bethge, and Wieland Brendel. Exemplary Natural Images Explain CNN Activations Better than State-of-the-Art Feature Visualization. In *Proceedings of the International Conference on Learning Representations (ICLR)*, 2021.
- [25] Roland S. Zimmermann, David Klindt, and Wieland Brendel. Measuring per-unit interpretability at scale without humans. In A. Globerson, L. Mackey, D. Belgrave, A. Fan, U. Paquet, J. Tomczak, and C. Zhang, editors, *Advances in Neural Information Processing Systems (NeurIPS)*, volume 37, pages 48448–48483. Curran Associates, Inc., 2024. doi: 10.52202/079017-1535. URL [https://proceedings.neurips.cc/paper\\_files/paper/2024/file/56ed2bd15b66f709cd81cb1aaa0496b9-Paper-Conference.pdf](https://proceedings.neurips.cc/paper_files/paper/2024/file/56ed2bd15b66f709cd81cb1aaa0496b9-Paper-Conference.pdf).
- [26] Julien Colin, Lore Goetschalckx, Thomas Fel, Victor Boutin, Thomas Serre, and Nuria Oliver. Choosing the right basis for interpretability: Psychophysical comparison between neuron-based and dictionary-based representations. *arXiv preprint arXiv:2411.03993*, 2024.
- [27] Avanti Shrikumar, Peyton Greenside, and Anshul Kundaje. Learning important features through propagating activation differences. In *Proceedings of the International Conference on Machine Learning (ICML)*, 2017.
- [28] Thomas Fel, Victor Boutin, Louis Béthune, Rémi Cadène, Mazda Moayeri, Léo Andéol, Mathieu Chalvidal, and Thomas Serre. A holistic approach to unifying automatic concept extraction and concept importance estimation. *Advances in Neural Information Processing Systems*, 36:54805–54818, 2023.

- [29] Lewis Smith, Senthoooran Rajamanoharan, Arthur Conmy, Callum McDougall, Tom Lieberum, János Kramár, Rohin Shah, and Neel Nanda. Negative results for saes on downstream tasks and deprioritising sae research (gdm mech interp team progress update #2. AI Alignment Forum, 2025.
- [30] Xiaoqing Sun, Alessandro Stolfo, Joshua Engels, Ben Peng Wu, Senthoooran Rajamanoharan, Mrinmaya Sachan, and Max Tegmark. Dense sae latents are features, not bugs. In *Mechanistic Interpretability Workshop at NeurIPS 2025*, 2025.
- [31] Thomas Fel, Thibaut Boissin, Victor Boutin, Agustin Picard, Paul Novello, Julien Colin, Drew Linsley, Tom Rousseau, Rémi Cadène, Lore Goetschalckx, Laurent Gardes, and Thomas Serre. Unlocking Feature Visualization for Deeper Networks with Magnitude Constrained Optimization. In *Advances in Neural Information Processing Systems (NeurIPS)*, volume 36, pages 37813–37826, 2023.
- [32] Vitali Petsiuk, Abir Das, and Kate Saenko. RISE: Randomized Input Sampling for Explanation of Black-box Models. In *Proceedings of the British Machine Vision Conference (BMVC)*, 2018.
- [33] Maximilian Dreyer, Erblina Purrelku, Johanna Vielhaben, Wojciech Samek, and Sebastian Lapuschkin. Pure: Turning polysemantic neurons into pure features by identifying relevant circuits. In *Proceedings of the IEEE/CVF Conference on Computer Vision and Pattern Recognition*, pages 8212–8217, 2024.
- [34] Bolei Zhou, Hang Zhao, Xavier Puig, Sanja Fidler, Adela Barriuso, and Antonio Torralba. Scene parsing through ade20k dataset. In *Proceedings of the IEEE conference on computer vision and pattern recognition*, pages 633–641, 2017.
- [35] Patrik O. Hoyer. Non-negative matrix factorization with sparseness constraints. *The Journal of Machine Learning Research (JMLR)*, 5(Nov):1457–1469, 2004.
- [36] Iliia Sucholutsky and Tom Griffiths. Alignment with human representations supports robust few-shot learning. *Advances in Neural Information Processing Systems (NeurIPS)*, 36:73464–73479, 2023.
- [37] Lukas Muttenthaler, Lorenz Linhardt, Jonas Dippel, Robert A Vandermeulen, Katherine Hermann, Andrew Lampinen, and Simon Kornblith. Improving neural network representations using human similarity judgments. *Advances in Neural Information Processing Systems (NeurIPS)*, 36:50978–51007, 2023.
- [38] Shobhita Sundaram, Stephanie Fu, Lukas Muttenthaler, Netanel Tamir, Lucy Chai, Simon Kornblith, Trevor Darrell, and Phillip Isola. When does perceptual alignment benefit vision representations? *Advances in Neural Information Processing Systems (NeurIPS)*, 37:55314–55341, 2024.
- [39] Lukas Muttenthaler, Klaus Greff, Frieda Born, Bernhard Spitzer, Simon Kornblith, Michael C Mozer, Klaus-Robert Müller, Thomas Unterthiner, and Andrew K Lampinen. Aligning machine and human visual representations across abstraction levels. *Nature*, 647(8089):349–355, 2025. doi: 10.1038/s41586-025-09631-6.
- [40] Jannis Ahlert, Thomas Klein, Felix A. Wichmann, and Robert Geirhos. How aligned are different alignment metrics? In *ICLR 2024 Workshop on Representational Alignment (Re-Align)*, 2024. URL <https://openreview.net/forum?id=ch1KB28bjV>.
- [41] Drew Linsley, Dan Shiebler, Sven Eberhardt, and Thomas Serre. Learning What and Where to Attend. In *Proceedings of the International Conference on Learning Representations (ICLR)*, 2019.
- [42] Thomas Fel, Ivan F Rodriguez Rodriguez, Drew Linsley, and Thomas Serre. Harmonizing the object recognition strategies of deep neural networks with humans. *Advances in Neural Information Processing Systems (NeurIPS)*, 35:9432–9446, 2022.
- [43] Martin N. Hebart, Charles Y. Zheng, Francisco Pereira, and Chris I. Baker. Revealing the multi-dimensional mental representations of natural objects underlying human similarity judgements. *Nature Human Behaviour*, 4(11):1173–1185, 2020.
- [44] Martin N. Hebart, Oliver Contier, Lina Teichmann, Adam H. Rockter, Charles Y. Zheng, Alexis Kidder, Anna Corriveau, Maryam Vaziri-Pashkam, and Chris I. Baker. THINGS-data, a multimodal collection of large-scale datasets for investigating object representations in human brain and behavior. *eLife*, 12:e82580, 2023. doi: 10.7554/eLife.82580.

- [45] Stephanie Fu, Netanel Tamir, Shobhita Sundaram, Lucy Chai, Richard Zhang, Tali Dekel, and Phillip Isola. DreamSim: Learning new dimensions of human visual similarity using synthetic data. *arXiv preprint arXiv:2306.09344*, 2023.
- [46] Fabian Gröger, Shuo Wen, and Maria Brbić. Revisiting the platonic representation hypothesis: An aristotelian view. *arXiv preprint arXiv:2602.14486*, 2026.
- [47] Iliia Sucholutsky, Lukas Muttenthaler, Adrian Weller, Andi Peng, Andreea Bobu, Been Kim, Bradley C Love, Erin Grant, Iris Groen, Jascha Achterberg, et al. Getting aligned on representational alignment. *arXiv preprint arXiv:2310.13018*, 2023.
- [48] Evan Hernandez, Sarah Schwettmann, David Bau, Teona Bagashvili, Antonio Torralba, and Jacob Andreas. Natural language descriptions of deep visual features. In *Proceedings of the International Conference on Learning Representations (ICLR)*, 2022.
- [49] Steven Bills, Nick Cammarata, Dan Mossing, Henk Tillman, Leo Gao, Gabriel Goh, Ilya Sutskever, Jan Leike, Jeff Wu, and William Saunders. Language models can explain neurons in language models. *OpenAI Blog*, 2023. URL <https://openaipublic.blob.core.windows.net/neuron-explainer/paper/index.html>.
- [50] Tuomas Oikarinen and Tsui-Wei Weng. CLIP-Dissect: Automatic description of neuron representations in deep vision networks. In *Proceedings of the International Conference on Learning Representations (ICLR)*, 2023.
- [51] Ming Li, Xin Chen, Xin Li, Bin Ma, and Paul MB Vitányi. The similarity metric. *IEEE transactions on Information Theory*, 50(12):3250–3264, 2004.

## A Limitations and broader impact.

**Limitations.** We acknowledge several limitations. First, our model-level analyses span only six architectures, which limits statistical power and makes it difficult to disentangle correlated properties of representations (*e.g.*, sparsity and coarse-grained alignment may co-vary across architectures). Second, almost all models are evaluated at ViT-B scale. This controls for scale across architectures, but whether the interpretability gap between supervised and foundation models persists or reverses at larger scales remains an open question. Third, we focus on a specific set of representational properties: downstream task performance, locality, and alignment with human similarity judgments. Other factors, such as training data or robustness, may also shape interpretability. Finally, our *nameability* protocol relies on external vision-language models to score the accuracy of human descriptions. This is imperfect: using an external model introduces its own biases and cannot provide a direct ground-truth measure of whether a description captures the feature. However, directly testing free-form descriptions against the evaluated vision foundation models is not currently possible, since these models do not provide a reliable way to judge whether a natural-language description matches one of their internal visual features. We therefore use external image–text similarity as a practical proxy, keeping the scorer fixed across all evaluated models so that its biases are held constant in the comparisons.

**Broader impact.** This work contributes to human-centered evaluation of model interpretability. By testing whether people can localize and describe decision-relevant features, our protocol adds to a broader effort to assess whether vision models are transparent enough for settings where human oversight matters, including critical applications. However, interpretability evaluations should not be taken as evidence of safety or reliability on their own. A model whose features appear more interpretable may still fail under distribution shift or behave unpredictably in downstream applications. Our results should therefore be viewed as one component of a broader evaluation ecosystem, complementing robustness, fairness, calibration, and task-specific validation.

## B Additional Related Work

**Representational alignment with human perception.** A growing body of work investigates how well DNN representations mirror human perceptual judgments [47], with parallel evidence that aligning model feature attributions with human importance maps improves object recognition [42]. Alignment with human similarity judgments has been shown to improve transfer [36, 37], though benefits are task-dependent: alignment helps retrieval but may hurt discriminative classification [38]. Crucially, Muttenthaler et al. [39] showed that this trade-off depends on granularity: coarse-grained and fine-grained alignment affect downstream tasks differently. While prior work treats alignment as a driver of task performance, we treat it as a potential correlate of *feature interpretability*—a connection that, to our knowledge, has not been investigated.

**Automated feature scoring with vision-language models.** Hernandez et al. [48] proposed labeling visual neurons with natural-language descriptions and measuring label quality via retrieval accuracy. Bills et al. [49] extended this idea to language model neurons, using GPT-4 to generate explanations scored by how well they predict held-out activations. CLIP-Dissect [50] matched each neuron to the most CLIP-similar concept from a large vocabulary, enabling scalable, open-vocabulary labeling without human annotation. Our *nameability* score builds on this spirit—participants describe a feature in free text and we measure CLIP cosine similarity between their description and feature-centered crops—while retaining the validity guarantee of human behavioral data.

## C Details about the control experiment

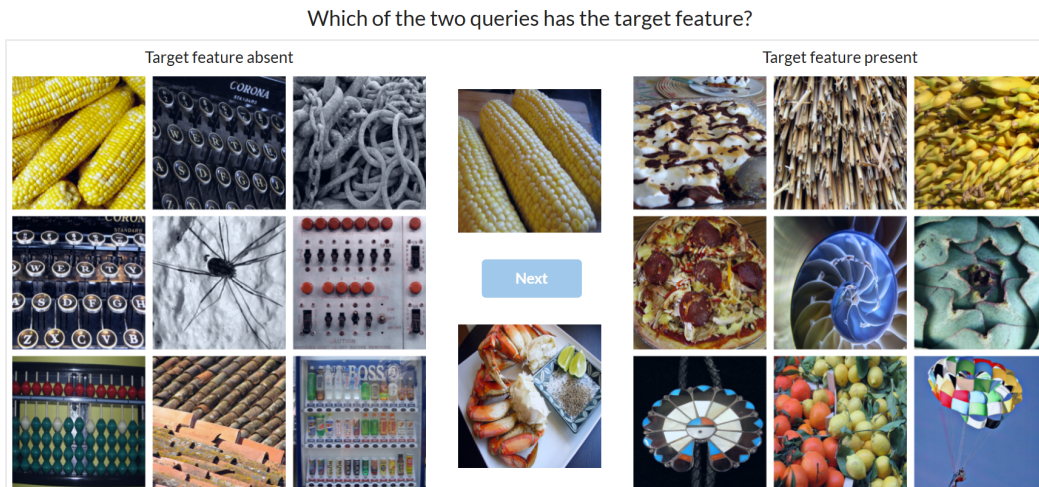


Figure A.1: Example of a trial from Zimmermann et al. [19]. In this protocol, the task is to pick the query image that matches the reference images illustrating the feature (left panel), by leveraging reference images that both highly activate the feature (right panel) and images that minimally activate it (left panel). In this example, the task can be trivially solved by relying on semantic grouping. By observation of the minimally activating stimuli (left panel), it is easy to conclude that the neuron of interest is not a corn detector, yet, it is hard to articulate what visual pattern is captured by the neuron (images in the right panel).

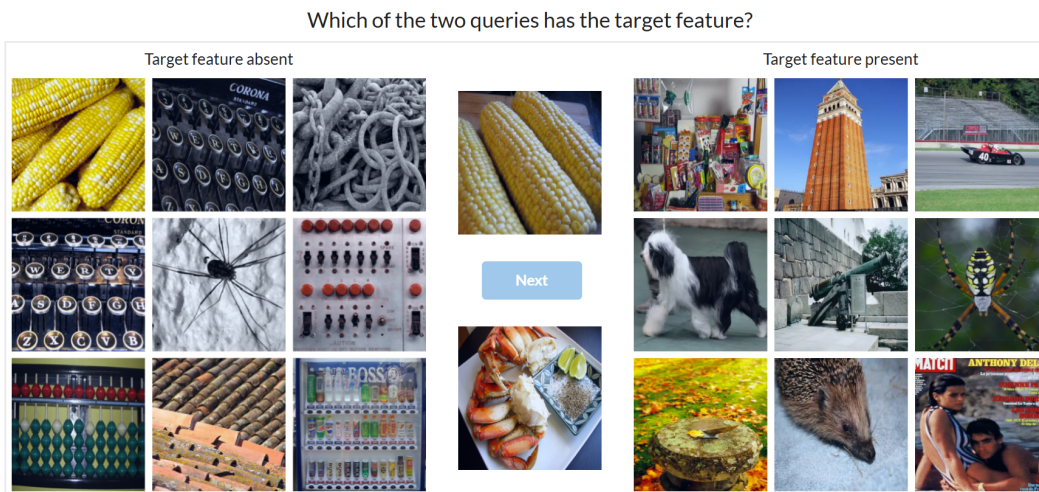


Figure A.2: Instantiation of the trial from Fig. A.1 in our control experiment (Sect. C). In this protocol, we replace the images that highly activate the feature with images that carry little to no information about the feature’s visual content. If the protocol only quantify the degree to which participant understand the feature, we expect them to perform at chance (50%) in this setup.

## D Scaling model interpretability

Model-level interpretability is a property of a model’s full feature population. Under a fixed annotation budget, we therefore face a choice: cover more features (*breadth*) or measure each feature more carefully (*depth*). This pilot asks which choice better approximates the population score.

**What we do.** We collect interpretability judgments on 80 DINOv2 neurons; this defines our reference score of 0.5555. We then use bootstrapping (200 resamples per design) to simulate two cheaper alternatives: subsampling fewer units (breadth) or reducing the number of images and trials per unit (depth). For each design we report the bootstrap mean and SD.

Strategy	Setting	Bootstrap score	$\Delta$ vs. ref.
Reference	All 80 units (full data)	0.5555	—
Breadth	10 units	$0.5586 \pm 0.0291$	+0.0031
Breadth	30 units	$0.5541 \pm 0.0142$	-0.0014
Breadth	60 units	$0.5552 \pm 0.0057$	-0.0003
Depth	1 image, 1 trial	$0.5475 \pm 0.0376$	-0.0080
Depth	1 image, 3 trials	$0.5484 \pm 0.0278$	-0.0071
Depth	10 images, 1 trial	$0.5509 \pm 0.0083$	-0.0046

Table A.1: **Breadth vs. depth under a fixed budget.** Bootstrap estimates of cheaper designs against the full-data reference. Breadth approaches the reference more quickly than depth.

**What we find.** Breadth converges quickly to the reference: 60 units already match it within  $\pm 0.006$ . On the other hand, depth converges more slowly. Even 3 trials on a single image ( $\pm 0.0278$ ) is less stable than 30 units alone ( $\pm 0.0142$ ).

**Why this points to scaling features.** Depth makes our estimate of the units we picked more precise; breadth makes it more representative. Because the 80-unit reference is itself a stand-in for a much larger feature population, only breadth moves the estimate toward what we actually care about. We therefore allocate the main experiment’s budget across as many features as possible rather than across repeated judgments on a small set of features.

## E Overview of our feature extraction and explanation pipeline

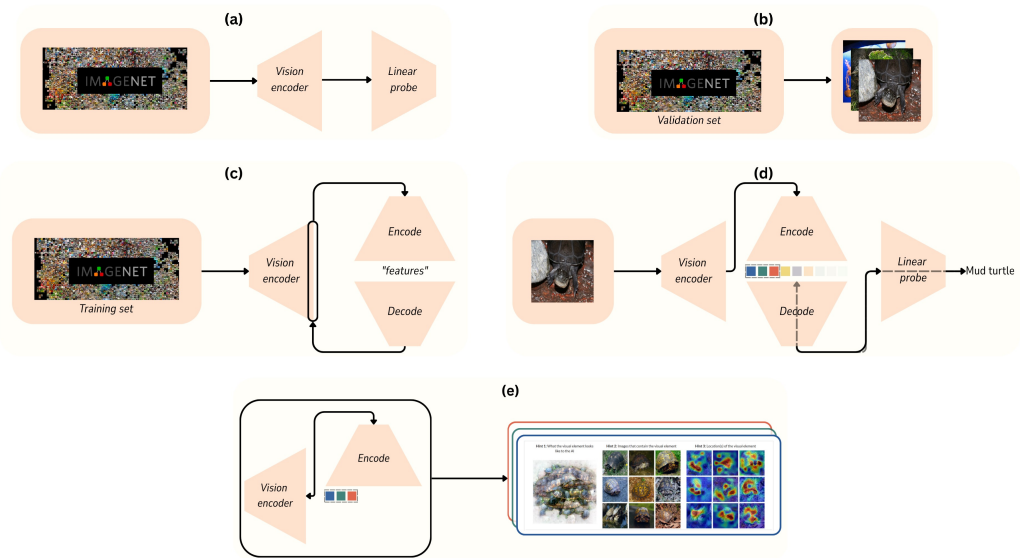


Figure A.3: **Pipeline for extracting and explaining vision model features.** (a) A linear probe is trained on ImageNet over the frozen backbone to derive per-feature importance and an accuracy baseline. (b) A representative subset of ImageNet images is selected to anchor evaluation across all models. (c) A TopK SAE is trained on patch-token activations to recover monosemantic features. (d) The most important features are selected per image, using Gradient×Input. (e) Each feature is explained via a MACO visualization [31], nine top-activating images, and RISE heatmaps [32]. See Section 3.2 for full details.

## F Distribution of feature reuse across models

Table A.2: Number of unique SAE features retained after filtering dense features for each model. Differences reflect varying degrees of feature reuse across architectures.

	Supervised		Foundation			
	ViT-S/16	ViT-B/16	DINOv2	DINOv3	CLIP	SigLIP
# Unique features	1012	1305	1119	1018	545	896

## G Psychophysics experiment

The experiment proceeded in three stages. Participants first read a welcome screen describing the task they were about to perform (Fig. A.4). They then completed a short practice session to familiarize themselves with the task, followed by the main experiment. On each trial, a feature was presented through its visualization, top activating images, and corresponding heatmaps; depending on the condition, participants were asked either to click on the location where they expected the feature to appear in a new image (*localizability*, Fig. A.5) or to provide a free-text description of the feature (*nameability*, Fig. A.6).

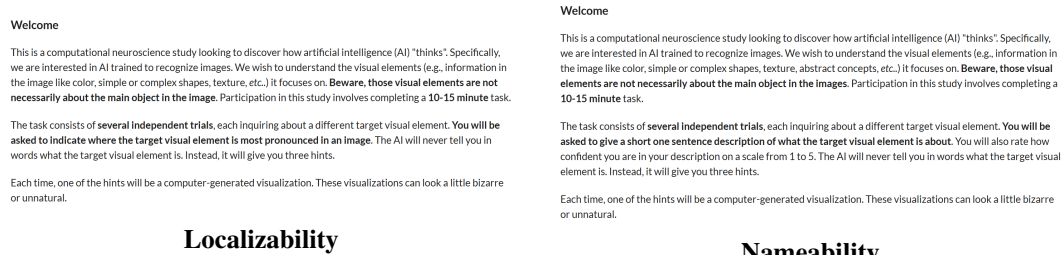


Figure A.4: Welcome screens shown to participants before the psychophysics experiments. Left: instructions for the *localizability* task. Right: instructions for the *nameability* task.

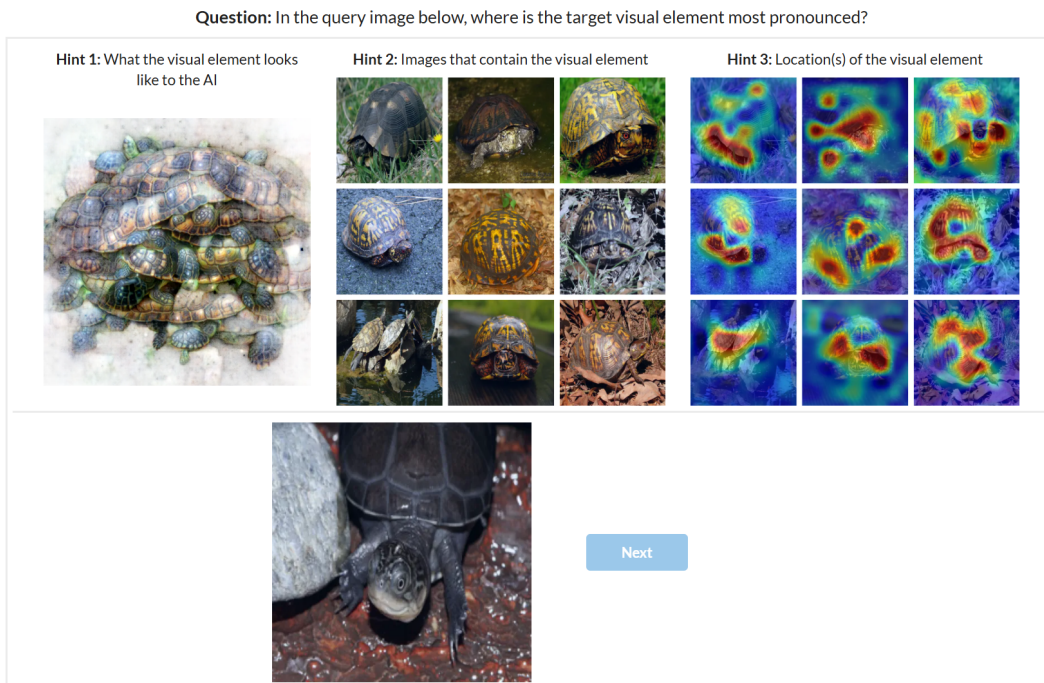




Figure A.5: Screenshot of a trial for the *localizability* experiment for DINOv3. A feature is explained through 3 panels at the top: (left) feature visualization by means of a maximally activating synthetic image, (middle) a set of images that highly activate the features, with their associated heatmaps (right) highlighting where the feature is located on those images. Participants were asked to click on a location where they expected the feature to be present on a new image (bottom). The more interpretable the feature, the more likely they are to correctly identify an area where the feature is present in the image.

Question: What is the target visual element about?

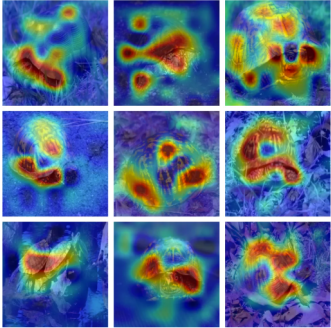
Hint 1: What the visual element looks like to the AI



Hint 2: Images that contain the visual element



Hint 3: Location(s) of the visual element



Write a short description of the target visual element.

Your confidence in the description

Low High

1 2 3 4 5

Next

Figure A.6: Screenshot of a trial for the *nameability* experiment for DINOv3. A feature is explained through 3 panels at the top: (left) feature visualization by means of a maximally activating synthetic image, (middle) a set of images that highly activate the features, with their associated heatmaps (right) highlighting where the feature is located on those images. Participants were asked to give a text-free description of what the feature is about (bottom). The more interpretable the feature, the more accurate their description.

## H Quadrant of features

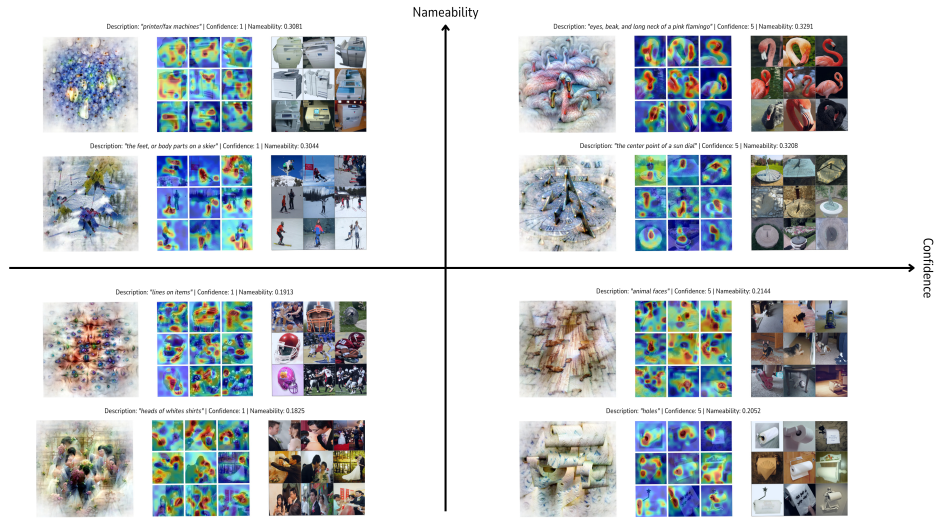


Figure A.7: **Relationship between *nameability* and *confidence* at the feature level.** Examples of features from each of the four quadrants defined by human-rated confidence (x-axis) and *nameability* (y-axis). For each feature we show, from left to right: the feature visualization, heatmaps for top activating images, and the top activating images. The header above each example reports the human-provided description together with its confidence and *nameability* scores. Features in the upper-right quadrant are both confidently and accurately named, whereas features in the lower-left are neither confidently nor accurately named.

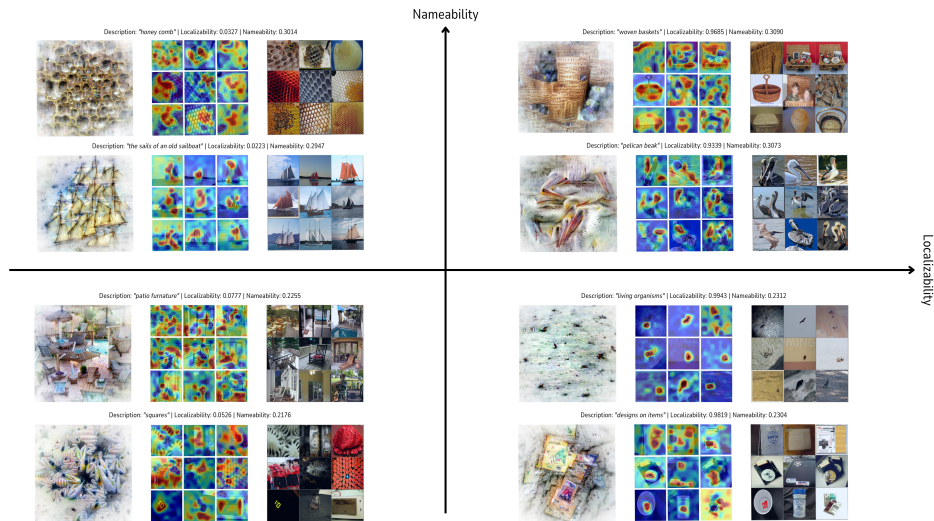


Figure A.8: **Relationship between *nameability* and *localizability* at the feature level.** Examples of features from each of the four quadrants defined by *localizability* (x-axis) and *nameability* (y-axis). For each feature we show, from left to right: the feature visualization, heatmaps for top activating images, and the top activating images. The header above each example reports the human-provided description together with its *localizability* and *nameability* scores. Features in the upper-right quadrant are both accurately localized and named, whereas features in the lower-left are not accurately localized or named.

## I Nameability details

**Crop vs full image** For a given feature, we evaluate both the similarity of a general description—the name of the main object, and a more specific one which we believe encapsulates the feature better. Descriptions that go beyond simply naming the main object in the image generally receive a higher score when using crops (see Fig. A.9 for an illustration).

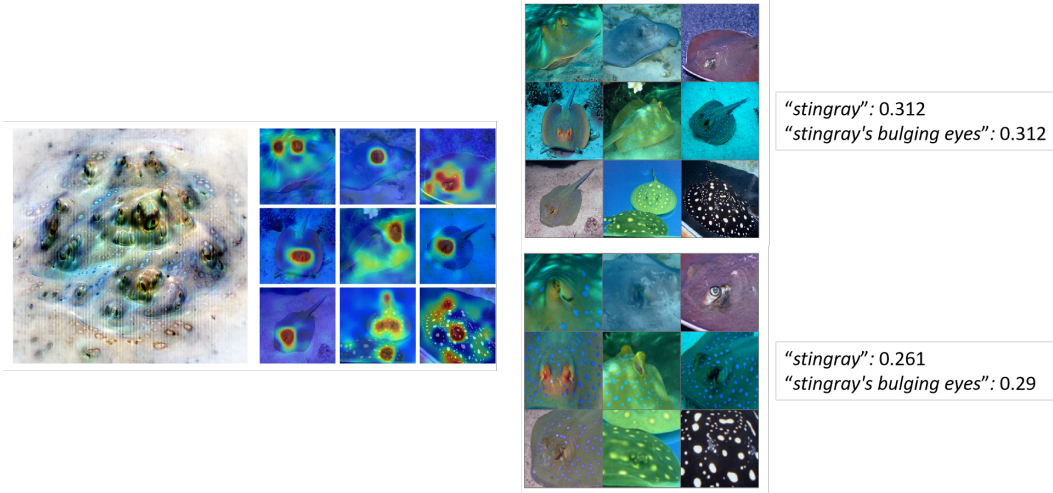


Figure A.9: For a given feature, we evaluate the similarity of two descriptions, a general one consisting of the name of the main object, and a more specific one which we believe encapsulates the feature better. Using crops allows us to reward descriptions that go beyond simply naming the main object in the image.

Regardless, Table A.3 highlights that results are fairly robust to the type of image used: *full images* vs. *crops*.

Table A.3: Nameability scores computed using the full image (bottom row) versus crops (top row) around the feature location. Best result per row is in bold, second best is underlined.

	Supervised		Foundation			
	ViT-S/16	ViT-B/16	DINOv2	DINOv3	CLIP	SigLIP
Crops (↑)	<b>0.274</b>	<u>0.273</u>	0.259	0.260	0.266	0.253
Full image (↑)	<u>0.276</u>	<b>0.277</b>	0.256	0.258	0.260	0.250

## J Detailed results for the psychophysics experiments.

Across both protocols, interpretability scores were non-normally distributed (Fig. A.10 and Fig. A.11) for every model (Shapiro–Wilk test,  $p < .001$ ). We therefore report the median score per model as a more representative measure of central tendency.

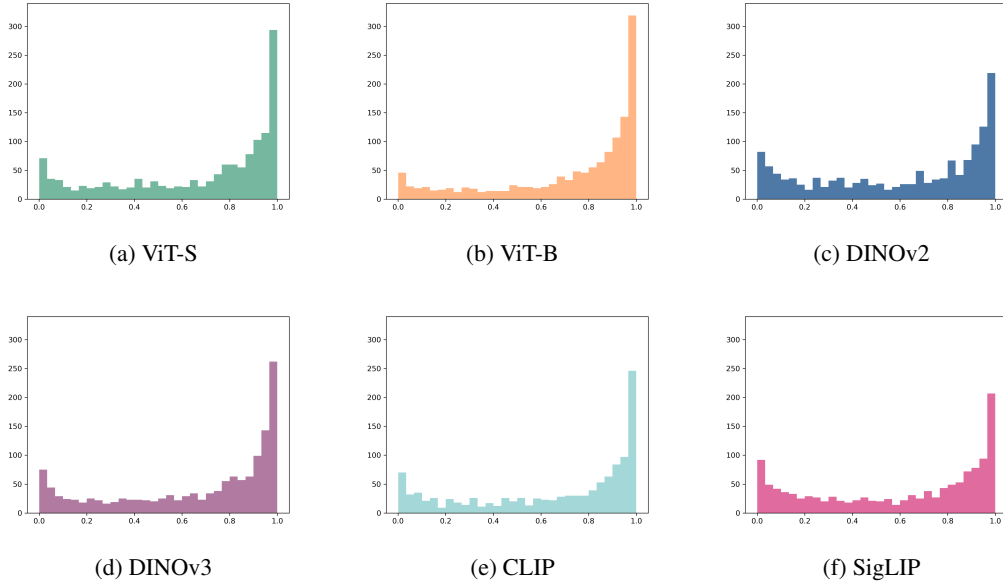


Figure A.10: **Distribution of feature *localizability* scores across models.** Each panel shows the distribution of *localizability* scores for one model.

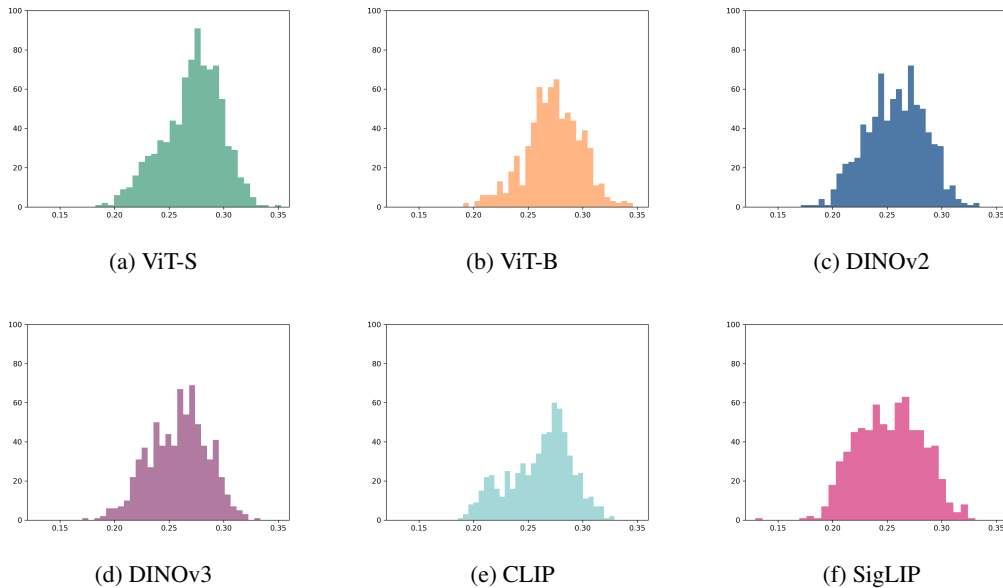


Figure A.11: **Distribution of feature *nameability* scores across models.** Each panel shows the distribution of *nameability* scores for one model.

## K Additional results on locality of representations

A feature can be considered local if it fires on a few grouped pixels, i.e., (i) *few* pixels are active and (ii) those active pixels are *spatially grouped*. The Hoyer sparsity used in Section 4.1 primarily targets the first component. As a complementary proxy for the latter, we use the **Kolmogorov complexity** [51] of each feature’s RISE heatmaps, approximated by their JPEG compressibility: the size of the losslessly compressed heatmap, normalized by its uncompressed size. Grouped activations form contiguous, redundant regions and compress well; scattered activations do not. Lower values therefore indicate more spatially grouped heatmaps. We average over the heatmaps of each feature’s nine most activating images and then over all features for a model.

**Results.** Across the six models, compressibility correlates with both interpretability protocols in the expected direction (see Fig. A.12)—interpretable models tend to have more compressible heatmaps—although neither correlation reaches significance: *localizability* ( $\rho = -0.63$ ,  $p = 0.178$ ) and *nameability* ( $\rho = -0.78$ ,  $p = 0.216$ ).

**Limitation.** Compressibility alone does not distinguish a heatmap with a single active pixel and a heatmap where every pixel takes the same value, as both are highly compressible. The score, therefore, captures the presence and, to some extent, the number of activation groups, but not whether those groups are spatially confined. We therefore read it as a useful complement to Hoyer sparsity: suggestive of grouping, but, on its own, an incomplete proxy for locality.

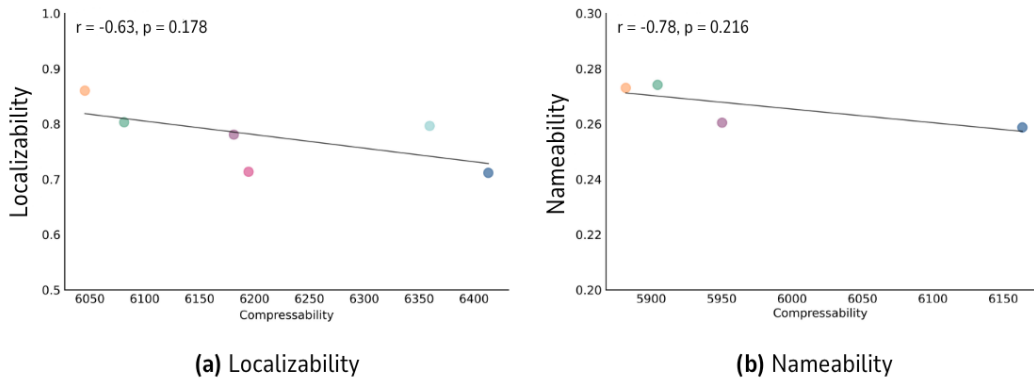


Figure A.12: **Compressibility of feature heatmaps as a complementary measure of locality.** Each panel plots an interpretability score against the mean compressibility of a model’s feature heatmaps (lower = more grouped activations). Left: *localizability*. Right: *nameability*. Spearman  $\rho$  and  $p$ -values shown per panel. Correlations point in the expected direction on both protocols but do not reach significance.

## L Additional results on alignment with human similarity judgments

The Levels dataset [39] provides human similarity judgment at three different levels, by constructing triplets using 3 images from 1 class to 3 different classes. For completeness, in this section we report results from the third triplet category beyond the coarse- and fine-grained ones reported in Section 4.2. In this *border-level* category, two images share the same ImageNet class while the third belongs to a different ImageNet class, probing a granularity that sits between fine and coarse similarity.

The Spearman correlations with border-level alignment fall between the coarse and fine-grained results, with positive but non-significant trends on both protocols (see Fig. A.13): *localizability* ( $\rho = 0.58$ ,  $p = 0.223$ ) and *nameability* ( $\rho = 0.72$ ,  $p = 0.11$ ). The pattern is consistent with interpretability tracking categorical alignment more closely than within-category alignment.

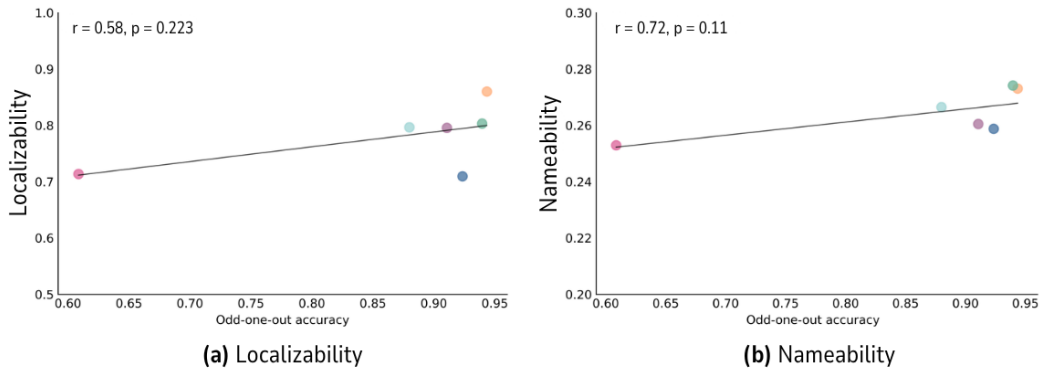


Figure A.13: **Border-level alignment on the Levels dataset.** Each panel plots an interpretability score against odd-one-out accuracy on the border-level triplets of Levels [39]. Left: *localizability*. Right: *nameability*. Spearman  $\rho$  and  $p$ -values per panel. Both correlations are positive but non-significant, sitting between the coarse- and fine-grained results.

## M Additional figures

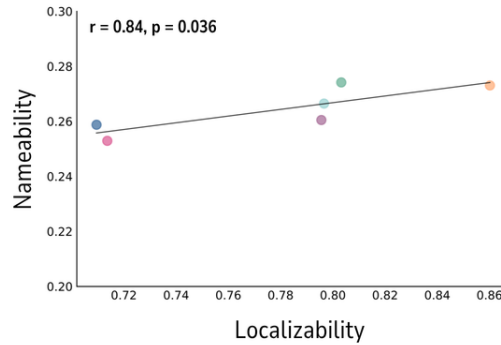


Figure A.14: **The two protocols converge on the same model ranking.** Median *nameability* plotted against median *localizability* across the six vision transformers. Despite differing in nearly every respect — pointing vs. writing, spatial heatmap vs. vision–language embedding — the two protocols produce a similar ranking of models, suggesting that we are measuring a stable property of the representation rather than an artifact of any one task.

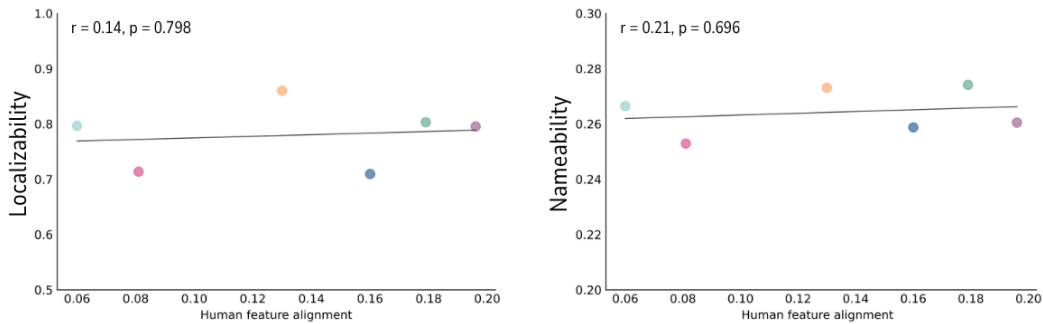


Figure A.15: **Alignment with human visual strategies does not predict interpretability.** Each panel plots an interpretability score against the overlap between model-driven and human-attended image regions [41, 42] across the six models. Left: *localizability*; right: *nameability*. Neither correlation is significant: a model can attend to the same image regions humans do and still encode what it sees there in features humans cannot readily make sense of.

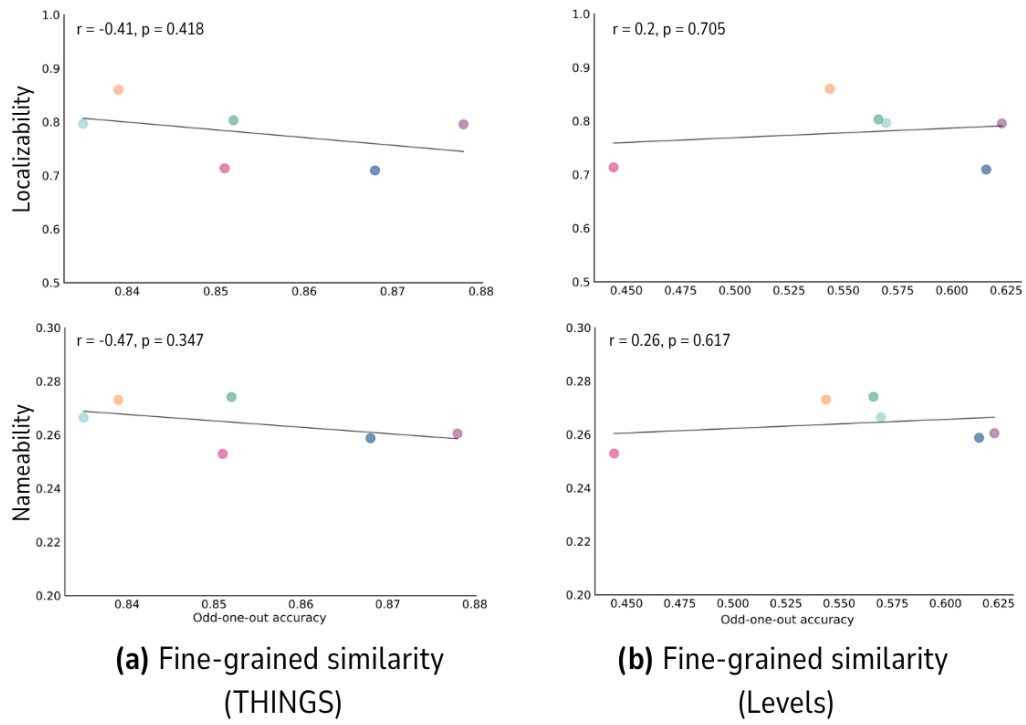


Figure A.16: **Alignment with fine-grained similarity does not predict interpretability.** Each panel plots an interpretability score against an alignment measure across the six models. Top row: *localizability*; bottom row: *nameability*. Columns: fine-grained alignment with human similarity judgments on THINGS [43] and Levels [39] (odd-one-out accuracy). Spearman  $\rho$  and  $p$ -values per panel. None of the four correlations reaches significance, suggesting that what matters for interpretability is not perceptual fidelity to fine visual details.